Enhanced $k_\parallel$ filtering effects in ballistic electron emission experiments

C. Strahberger[*]

Walter Schottky Institut und Physik Department, Technische Universität München, Am Coulombwall, 85748 Garching, Germany

J. Smoliner,[†] R. Heer, and G. Strasser

Institut für Festkörperelektronik und Mikrostukturzentrum der Technischen Universität Wien, Floragasse 7, A-1040 Wien, Austria

Double barrier resonant tunneling diodes (DBRTD's) buried below an Au/GaAs interface usually lead to a linear increase in the spectra obtained in ballistic electron emission microscopy/spectroscopy experiments. If grown directly below the Au/GaAs interface the spectrum changes to a clear steplike shape, which has been attributed to lateral wave-vector $k_\parallel$ filtering effects. In this paper, this assertion is tested and quantified by a systematic theoretical study of these structures in terms of a coherent scattering approach as well as magnetotunneling experiments. The calculations show that the enhanced $k_\parallel$ filtering is a result of the disordered Au/GaAs interface. The filtering effect is only observed for DBRTD's grown directly beneath the Au/GaAs interface. It vanishes if the DBRTD's are capped with 10 nm or more of GaAs. The calculated $k_\parallel$-filter width agrees well with the Shubnikov−de-Haas-like oscillations obtained from magnetotunneling experiments.

I. INTRODUCTION

Tunneling of electrons through interfaces of materials with strongly different electronic structures, e.g., a metal on a semiconductor, are, in spite of much research, presently not very well understood. Especially in the case of nonepitaxial interfaces, the degree to which energy and the lateral wave-vector $k_\parallel$ are conserved or randomized at the interface is still under discussion.[1–3] Furthermore, interface states effects have mostly been neglected. An excellent method of studying properties of these interfaces with a high lateral, as well as energetic resolution, is ballistic electron emission microscopy (BEEM) in conjunction with a probing heterostructure buried below the interface.

Ballistic electron emission microscopy (BEEM)[4,5] is a three-terminal extension of scanning tunneling microscopy (STM), where hot electrons are injected into a semiconductor via a thin metallic base layer. Originally used to determine Schottky barrier heights,[6–9] BEEM is now frequently used to study buried interfaces in semiconductor heterostructures.[10] On buried In$_x$Ga$_{1-x}$As/GaAs interfaces, misfit dislocations[11] were investigated by BEEM as an alternative to cathodoluminescense experiments, which were traditionally used for this purpose. Besides structural properties of buried interfaces, interface band-structure effects were investigated too. A good example of such an experiment is the determination of the GaAs/Al$_x$Ga$_{1-x}$As band offsets as a function of aluminum concentration[12] and the determination of the energetic position of higher conduction bands in AlAs.[6]

Instead of probing the buried structure itself, the latter can be used as a highly selective filter, which makes it possible to analyze the energy/$k_\parallel$-space distribution of the impinging electrons. In this paper, we used a double barrier resonant tunneling diode (DBRTD) on GaAs/Al$_x$Ga$_{1-x}$As basis to study the nonequilibirium distribution of electrons passing an Au/GaAs interface. To obtain a deeper understanding of the observed phenomena we performed a multiband, multichannel calculation based on the Landauer-Büttiker formalism[13,14] within the semiempirical tight-binding framework.[15–18] Calculations[19,20] relying on the same electronic model were performed to clarify the origin of the unexpected high-lateral resolution obtained by BEEM on Au/Si heterointerfaces.

This paper is organized as follows: In Sec. II, the basic scheme of the experiment is outlined, as well as the fabrication of the samples. Section III describes briefly the theoretical model. In the main part, Sec. IV, the experimental, as well as theoretical results, are presented and discussed. Finally this paper is concluded in Sec. V.

II. EXPERIMENTAL SETUP

The structures we studied experimentally, as well as theoretically, are double barrier resonant tunneling diodes (RTD) grown by molecular beam epitaxy on a GaAs substrate. The precise layer sequence is as follows: On a semi-insulating GaAs (001) substrate, an n-doped GaAs collector region ($d = 1\,\mu\text{m}, \text{N}_\text{D} = 1 \times 10^{18}\,\text{cm}^{-3}$) layer was grown, followed by a 150 nm spacer of undoped GaAs to provide a high-internal sample resistance. On top of these layers, the GaAs/Al$_{0.4}$Ga$_{0.6}$As double barrier RTD was grown and protected by a GaAs cap. The barriers are each 3.7 nm thick and enclose a 3 nm wide GaAs well. To keep the resulting I-V characteristic as simple as possible, the well width was designed to contain only a single quasibound state.

To prepare the samples for BEEM, an In/Sn collector contact was first alloyed in forming gas atmosphere. Then, the samples were dipped into hydrochloric acid (35%) to remove the thin native oxide layer. Finally, an Au film (7.5 nm) was evaporated via a shadow mask. All measurements were carried out at a temperature of T=4.2 K and a tunneling current of 5 nA. Note, however, that due to scattering events in the Au base and the band-structure misfit, the actual collector current is much smaller.

A band-edge diagram of this structure is shown in Fig. 1 together with the schematic view of the experiment.
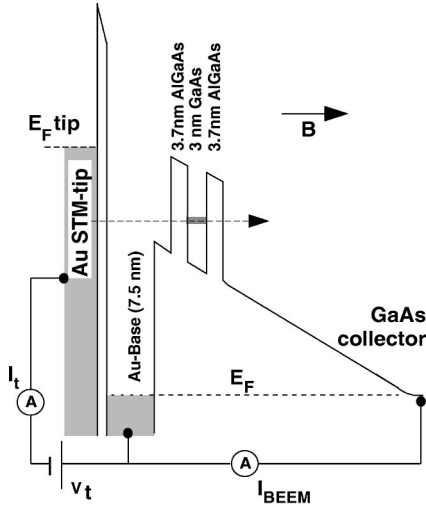
FIG. 1. View of the experimental setup together with a schematic view of the self-consistently calculated conduction-band profile of the structure. The direction of the additional magnetic field in Sec. IV C is also indicated.

III. THEORETICAL APPROACH

To model the BEEM experiment, we performed a multiband, multichannel ballistic transport calculation. The transport itself is regarded as a scattering process between two reservoirs, which are assumed to remain in thermodynamical equilibrium. By solving the Schrödinger equation of the whole device with appropriate boundary conditions,[21,17,18] it is possible to calculate the probability for an electron of the emitter with energy E, lateral wave-vector $\mathbf{k}_\parallel$, and normal wave-vector $k_{\perp,j}$ to tunnel into a propagating state with the quantum numbers $(E,\mathbf{k}_\parallel,k'_{\perp,i})$ of the collector. The indices $i,j=1,2,\ldots$, run over all Bloch states for fixed $(E,\mathbf{k}_\parallel)$ of the left and right reservoir, respectively. The electronic structure itself is calculated within the empirical tight-binding model,[22] which provides a realistic, as well as physically transparent, description of the band structure. Since this is a fully quantum-mechanical description on an atomistic basis, all important (single-particle) effects are taken into account. The tight-binding parameters for GaAs/AlAs and Au are given in Refs. 23 and 24, respectively. The self-consistently calculated local electrostatic potential $\Phi(\mathbf{r})$ as well as experimental band offsets and the Schottky barrier height are incorporated through the substitution of the orbital ("on-site") energies:[25]

$$E_\alpha \rightarrow E_\alpha - e\Phi(\mathbf{r}). \qquad (1)$$

The index α labels the basis atom, as well as the corresponding orbital.

Once the transmission coefficients $T(E,\mathbf{k}_\parallel,k_{\perp,j}\rightarrow k'_{\perp,i})$ have been calculated for a dense enough mesh in the Hilbert subspace of all possible *in* states, the current density through the heterostructure can be calculated using a Landauer-Büttiker-type expression:[13,14,26]

$$j = \frac{-e}{4\pi^3\hbar}\int_{BZ} d^2k_\parallel \, dE \sum_{i,j} \left[f_L(eV_t+E) - f_R(E) \right]$$
$$\times T(E,\mathbf{k}_\parallel,k_{\perp,j}\rightarrow k'_{\perp,i}). \qquad (2)$$

The integration runs over the projection of the Brillouin zone in growth direction and over energy. The integrand is proportional to the difference of the Fermi distributions f of the emitter and the collector. The potential difference between the STM tip and the base is denoted by V_t.

A more complete description of the method can be found in Refs. 21,17,18. Before proceeding to the results we briefly discuss the specific model, its relation to effective-mass calculations, and the involved approximations.

Since all measurements were performed at helium temperature and at very low-collector currents (<1 pA) inelastic processes, as well as electron-electron interaction are neglected. Furthermore, electrons that lose energy in the Au base cannot enter the GaAs region and thus, do not contribute to the BEEM current. This observation led to the assumption that the relevant physics can be described by assuming that electrons enter the GaAs cap layer from a Au band structure promoted by eV_t. In this way, the STM tip enters the model via its emission spectrum. To test the influence of the Au band structure on the tunneling current, the Au band structure was shifted rigidly upwards while leaving the Fermi energy constant. This had only a negligible effect on the tunneling current. Thus, the Au has the rather passive role of providing electrons for a wide range of $(E,\mathbf{k}_\parallel)$ states below Fermi level. The implicit assumption of planar tunneling results in current/voltage characteristics that are in good agreement with experimental data. Only electrons with a very large lateral wave vector, i.e., those tunneling at high biases through the L and X valley of $Al_xGa_{1-x}As$, seem to be more pronounced than experimentally observed. The same effect is observed in other models[5,27–29] that assume $\mathbf{k}_\parallel$ conservation.

To include effects from alloying and the nonepitaxial Au/GaAs interfaces, the lateral periodicity was broken down to that of a 3×1 and 2×2 lateral superlattice. Consequently, the conservation of $\mathbf{k}_\parallel$ is relaxed to that of the corresponding superlattice wave vector. Within the fist two monolayers of the GaAs cap, Au atoms were placed randomly in a few interstitial sites. Due to the high-computational effort involved, the calculation was confined to small unit cells. Nevertheless, a fully atomistic multiband calculation that incorporates elastic $\mathbf{k}_\parallel$-scattering effects from nonepitaxial and alloyed interfaces could be performed.

A further effect that influences the BEEM spectrum is the image charge effect, which lowers the Schottky barrier and shifts its maximum into the semiconductor. To see whether the inclusion of this effect is necessary, BEEM spectra for a DBRTD located 4 nm below the Au/GaAs interface have been calculated with—and without it. It turned out that due to the moderate electric field within the semiconductor, the onset Voltage increases by less than 10 meV and the current density grows in the linear regime by about 15%. Since the tunneling area is unknown and the effective Schottky barrier

height is determined from the BEEM experiment, it is safe to neglect the Schottky effect altogether.

Most theoretical descriptions of the BEEM spectra in literature are based on the effective-mass model, because it allows an analytic description. Already the treatment in the pioneering papers by Kaiser and Bell[4,5] yields a theoretical current that matches the experimental data to a very high degree.

Nevertheless, this agreement is partly due to the six fitting parameters that are—apart from an overall scale factor and the Schottky barrier height—the energetic separation of the Γ, L, and X valleys and their effective-mass ratios. While the energetic separations of the valleys are in overall agreement with the data obtained by other methods their relative effective masses differ significantly from accepted values. Furthermore, some of these key values show a considerable local variation due to strain and other lattice imperfections.

Since BEEM spectra are very sensitive to these, a theory that uses less fit parameters will generally have a poorer quantitative agreement. Thus, although the energetic separations of the valleys and their corresponding masses of the $sp^3d^5s^*$ tight-binding model used in this paper match both experiments and pseudopotential calculations quite well,[23] the resulting valley currents differ from measurement. However, the qualitative physics emerges naturally so that this model can be used as a starting point for effects such as interface scattering and valley-to-valley transfers on an atomistic level, which otherwise would have to be added *ad hoc*.[2,30] Consequently, at the expense of quantitative agreement, it is possible to many physical phenomena.

IV. RESULTS

A. Buried GaAs/AlGaAs RTD

The first structure we focus on are RTD's with a 10 nm GaAs cap between the top barrier and the Au contact. RTD's with a cap layer of 10 nm are referred to as ''buried RTD's'' while those with a much thinner cap layer as ''subsurface RTD's.'' As in previous studies,[4,5] a linear increase of the BEEM current above some threshold tip voltage is observed. At this bias, electrons from the Fermi level of the STM tip are energetically aligned with the RTD resonance level. A further restriction to the propagation imposed by the strongly differing effective masses between Au and GaAs. In consequence, the metal semiconductor interface acts effectively as a filter for the lateral wave-vector $\mathbf{k}_\parallel$: Only electrons close to $\mathbf{k}_\parallel = (0,0)$ propagate in the GaAs conduction bands. The wave function of electrons with larger lateral wave vectors are damped exponentially in GaAs. With increasing STM-bias V_t, electrons with a higher energy are injected into the conduction band and can have correspondingly larger $\mathbf{k}_\parallel$ components.

In our previous work, we were already able to give a semiquantitative explanation of the linear increase of the BEEM current by using a modified Bell-Kaiser model[31] within the framework of an effective-mass theory. The results of the tight-binding calculations are discussed below.

Figure 2 compares the theoretical (solid and dashed line) and the experimental (crosses) results for this structure. The
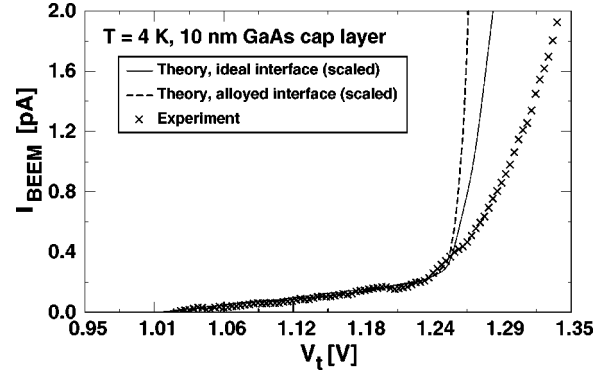

FIG. 2. BEEM current at 4.2 K as a function of V_t. The RTD is covered with a 10 nm GaAs cap layer. The continuous (dashed) line is a calculation assuming an ideal (alloyed) Au/GaAs interface, while the crosses show the measurement.

solid line was calculated assuming an ideal Au/GaAs interface, while for the dotted curve Au interstitials atoms were randomly placed in the first two monolayers of the GaAs cap. Interestingly, the linear increase in the current-voltage characteristic is not affected by the inclusion of an alloyed interface. Nevertheless, due to the increased scattering at the Au/GaAs interface, the current density is decreased. Note that due to the assumption of planar tunneling in Sec. III a comparison of the absolute current with the experiment is not possible. Both experiments and theoretical data show the expected linear increase in the current above the threshold voltage. At higher voltages, the onset of tunneling across the L valleys of the $Al_{0.4}Ga_{0.6}As$ barriers leads to a further increase in the slope.

To shed some light on how the current is distributed over $\mathbf{k}_\parallel$ space, we calculated the integrated and weighted transmission coefficient

$$T'(\mathbf{k}_\parallel) = \int dE \sum_{i,j} [f_L(eV_t + E) - f_R(E)]$$

$$\times T(E, \mathbf{k}_\parallel, k_{\perp,j} \rightarrow k'_{\perp,i})$$

for several STM-biases V_t. The two Fermi distributions were taken at 4 K. The result is shown as a function of the lateral wave vector along the $K - \Gamma - K$-Line in Fig. 3. Interestingly, the maximum remains at zero $\mathbf{k}_\parallel$ for all applied biases. Note, however, that the largest contribution to the current comes from electrons with a small, but nonzero $\mathbf{k}_\parallel$, since the missing two-dimensional wave-vector integration introduces an effective weight factor of $|\mathbf{k}_\parallel|$. As mentioned above, the $\mathbf{k}_\parallel$ distribution broadens with increasing V_t. This broadening is a result of the increased total-energy E of the electrons, which allows a larger $\mathbf{k}_\parallel$ value according to $E = E_{res} + \hbar^2 k_\parallel^2 / 2m^*$. The effective electron mass in the GaAs well and its resonance energy are denoted as m^* and E_{res}, respectively. This picture does not change for the alloyed interface.

B. Subsurface GaAs/Al$_x$Ga$_{1-x}$As RTD

An interesting situation occurs when the protective GaAs cap layer is thinned down to only ca. 4 nm. As reported
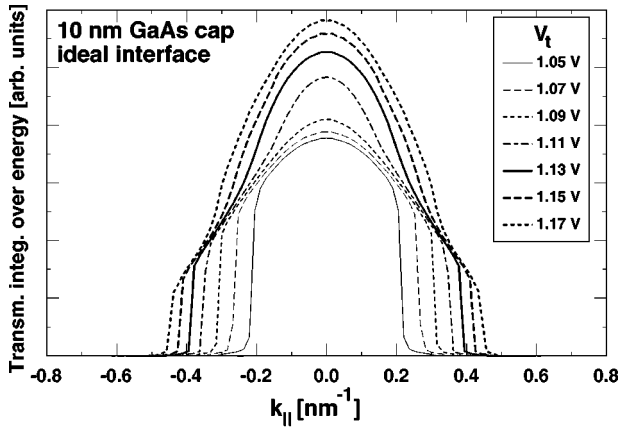
FIG. 3. Calculated cumulative transmission probability of this structure from Fig. 2 as a function of $\mathbf{k}_\parallel$ along the $K-\Gamma-K$ line for several values of V_t. Distributions for the ideal and the alloyed interface differ only in a constant factor.

FIG. 5. Calculated BEEM spectra for subsurface DBRTD's with an ideal Au/GaAs interface and a capping of 3, 4, and 5 nm GaAs, respectively.

previously,[1] experiments reveal a step-like current voltage characteristic as it is shown by the dotted curve in Fig. 4. This characteristic shape can be found in various subsurface RTD structures,[1] although it seems to be more pronounced in conjunction with narrow energy filters.

Applying the above tight-binding model with an ideal Au/GaAs interface to this case, one still retains the linear current increase with a slightly later onset at roughly 1.08 V. The fact that the onset is shifted to higher biases can be readily explained with Fig. 1: A thinner cap implies a smaller voltage drop between the Au/GaAs interface and the RTD and therefore a relative up-shift of the resonance level. The linear increase is in accordance with effective-mass calculations, but clearly deviates from the experimentally found sublinear slope. Furthermore, there is no trace of interferences in the cap layer, which would be a possible explanation of the observed sublinear slope. Sweeping the cap layer thickness from 3 through 5 nm GaAs does not affect the characteristic linear behavior (cf. Fig. 5). In this way, interferences can be ruled out.
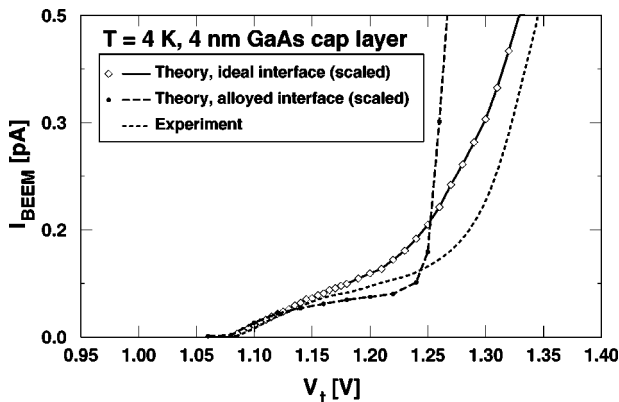

FIG. 4. BEEM spectrum for a subsurface DBRTD. The dotted line shows the experimental data, while the solid (dashed) curve is a calculation assuming a perfect (alloyed) Au/GaAs interface, respectively.
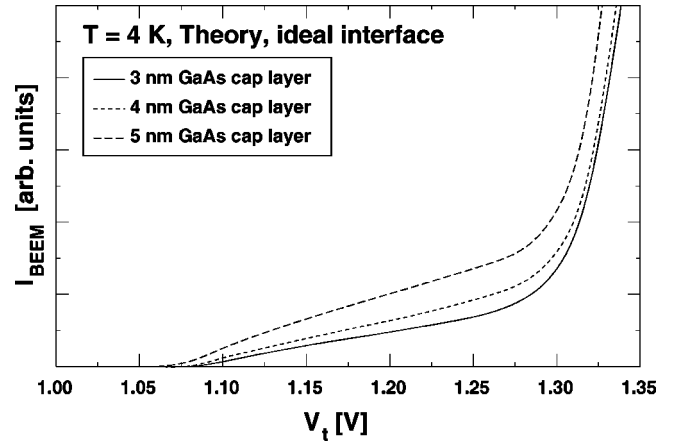
For all spectra in Fig. 5 a defect free and clearcut Au/GaAs interface was assumed, which is obviously a highly idealized picture of the actual situation: Among other investigations, BEEM studies[32,33] have shown that Au/GaAs interfaces are not perfect and even at room temperature, Au diffuses quickly more than two monolayers deep into the sample.[32,34] Moreover, an outdiffusion of Ga or As atoms into the gold can occur so that a considerable amount of disorder can be expected at the Au/GaAs interface. Since the actual interface morphology is unknown, the Au atoms were assumed to be randomly distributed over few of the interstitial sites of the first two monolayers of the GaAs cap. This is done as described in Sec. III by modeling this interface with a lateral superlattice. This arrangement relaxes the $\mathbf{k}_\parallel$ conservation to that of the corresponding superlattice wave vector. Since the interstitials have (in this model) no internal degree of freedom, the transmission remains fully elastic. Although the modification of the physical model is rather weak, the resulting effect is profound. Figure 4 compares the calculated current-voltage characteristics for an alloyed interface (dashed line) with those for an ideal interface (solid line) and the experimental data (dotted line). Due to scattering, the current density has decreased. To compare both curves with experimental data the current has been scaled so that the initial slopes match. The onset bias of the BEEM current is unaffected by the interstitials, while for V_t larger than ca. 1.10 V, the calculated current clearly deviates from the initial linear increase. In accordance with the experiments, we see a slow, but nonzero further increase of the current. The sharp rise at roughly 1.25 V stems from electrons tunneling over the $Ga_xAl_{1-x}As$-L valleys. Different distributions of the interstitials and a different shape (2×2) of the super cell have been tested, but the qualitative behavior remains unaffected. However, we want to point out that these comparatively small lateral superlattices can only mimic the situation of the completely aperiodic and randomized interface. The introduction of scatterers just below the interface leads to a redistribution of the electrons into the side valleys of GaAs and consequently to an enhancement of the L-valley current relative to the Γ-valley contribution. This effect is believed to
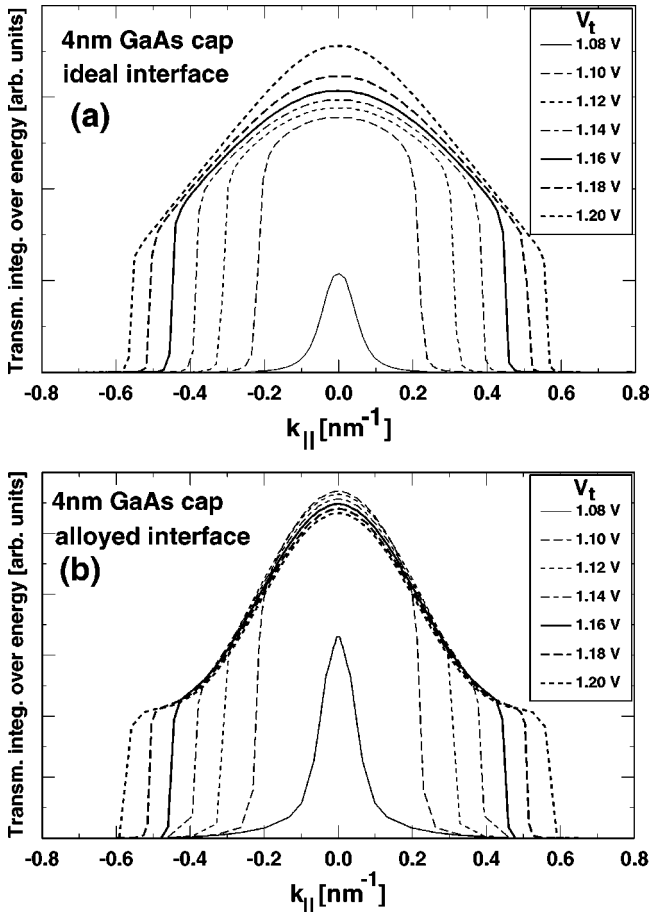
FIG. 6. Transmission probability of a subsurface DBRTD integrated over energy as a function of the lateral wave vector along the $K-\Gamma-K$ line. In part (a) an ideal Au/GaAs interface was assumed, while part (b) shows the corresponding distribution for an alloyed interface.

stem from the sheer number and large effective masses ($m_t \approx 1.9\,m_e$, $m_l \approx 0.13\,m_e$) of the L valleys and is in accordance with effective-mass calculations performed by Smith *et al.*[30]

The distribution of the current in $\mathbf{k}_\parallel$ space changes characteristically with the type of interface: In comparison with the distribution for an ideal interface, which is shown in Fig. 6(a), the larger $|\mathbf{k}_\parallel|$ values are suppressed in the alloyed structure [Fig. 6(b)] for V_t larger than 1.10 V. At this bias, a deviation from the linear increase is observed (cf. Fig. 4). Even more pronounced is this effect for a larger super cell: The same calculation for a 2×2 superlattice yielded a sharp cutoff at $|k_\parallel| \approx 0.17$ nm^{-1} (cf. Fig. 7). This asserts that the step is due to enhanced $\mathbf{k}_\parallel$ filtering and can be easily understood from the property of a $\mathbf{k}_\parallel$ filter: Since the electrons are confined to mostly low-$\mathbf{k}_\parallel$ values, an increase in the bias does not result in a larger number of electrons that are able to tunnel resonantly.

Since the step vanishes when the DBRTD is buried deeper into the GaAs, a proportion of the transmitted electrons must tunnel through quasilocalized states generated by the interstitials. When the Au/GaAs alloy is close to the DBRTD the interface states will couple to the quasibound state of the RTD and electrons are able to tunnel resonantly
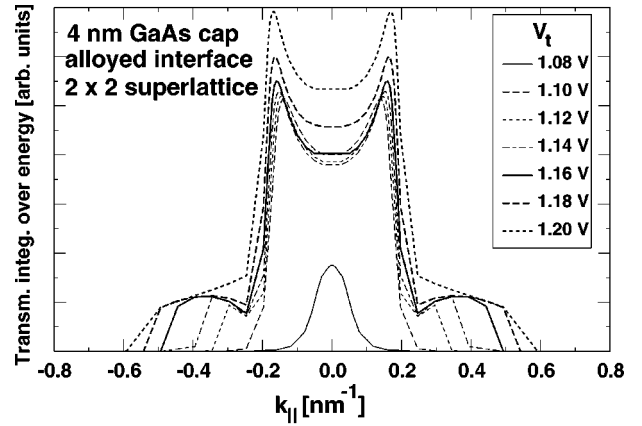

FIG. 7. Same as Fig. 6(b), but for a 2×2 lateral superlattice. The double-maximum results from the (artificial) band-structure folding.

via this path. The Au atoms in the intermixed interface have no periodicity, thus, the corresponding states have no or only a small ''dispersion'' leading to an additional energy/$\mathbf{k}_\parallel$ filter for electrons tunneling though them.

C. Magnetotunneling

To further test the $\mathbf{k}_\parallel$-filtering property of subsurface DBRTD, BEEM spectra were studied as a function of the magnetic field applied parallel to the tunneling current (cf. Fig. 1). Figure 8(a) shows typical BEEM spectra measured at various magnetic fields. Several features are evident: At $B=0$ T (curve 1), the BEEM current is zero below $V_t =1.05$ V, which corresponds to the situation, where the Fermi level in the tip is aligned with the resonant level inside the double barrier structure. Between $V_t=1.05$ V and $V_t =1.25$ V, which means as long as the Fermi level in the tip is below the Al$_x$Ga$_{1-x}$As barrier height, a step-like feature is observed. For higher-bias values, the barrier height is overcome and the ballistic current increases strongly. With increasing magnetic field, the spectral behavior appears to be unsystematic. To illustrate this, three typical curves for high-magnetic fields are shown. At 2.6 T (curve 2), the step-like feature has disappeared and the current is always smaller than at zero magnetic field. Already at B=3 T (curve 3), the step is well-pronounced again and the BEEM current is enhanced compared to the $B=0$ T spectrum. At 8.15 T (curve 4), the step is weak and the ballistic current is generally reduced compared to the $B=0$ T spectrum but larger than for the $B=2.6$ T spectrum. In addition, the step is shifted to higher bias. Note that this influence of the magnetic field is only observed at liquid-helium temperatures. At $T=100$ K, the BEEM spectra no longer change with increasing magnetic field.

The BEEM current was also investigated as a function of magnetic field keeping the tunneling bias V_t constant. For this purpose, a set of BEEM spectra was measured at various magnetic fields, keeping B constant during the measurement. This procedure was chosen, because the tip position is drifting in magnetic fields due to magnetostriction effects in the scanning piezo. To make sure that all spectra are measured at
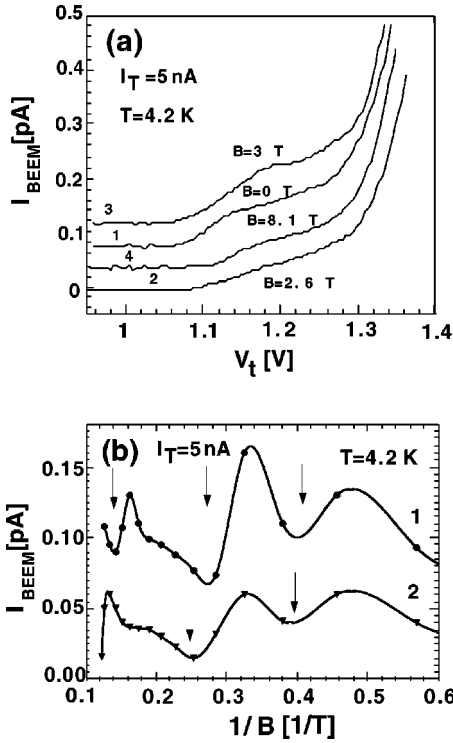
FIG. 8. In part (a) the curves one through four show the BEEM spectra measured at applied magnetic fields of 0, 2.6, 3, and 8.16 T, respectively. The direction of the magnetic field B is given in Fig. 1. All measurements were carried out at T=4.2 K and a tunneling current of 5 nA. An offset was added to the spectra for better clarity. Part (b) shows the BEEM current as a function of the reciprocal magnetic field for the STM biases of $V_t = 1.25$ V (curve 1) and $V_t = 1.15$ V (curve 2). The solid lines are a guide to the eye. Arrows indicate pronounced minima.

the same position, images were taken before each spectrum. The tip position was then corrected manually taking a prominent topographic structure as reference point. In Fig. 8(b), the BEEM current is plotted as function of the magnetic field for tunneling voltages of $V_t = 1.25$ V (curve 1) and $V_t = 1.15$ V (curve 2), respectively. Plotted as a function of the inverse magnetic field, the data exhibit an oscillatory behavior in $1/B$ and the most pronounced minima are marked by arrows. Comparing both curves, it is obvious that all minima positions are shifted if the STM bias is changed and the shift increases with increasing magnetic field. The bias dependence of the minima positions immediately explains the apparently unsystematic B-dependent behavior of the BEEM spectra: Each point of the BEEM spectrum oscillates at its own frequency in $1/B$, and therefore, no obvious magnetic-field dependence can be observed in the spectra directly.

As a result from Sec. IV B subsurface RTD's are a momentum filter for electrons around $k_\parallel = 0$. In other words, only electrons around $E_\parallel = \hbar^2 k_\parallel^2 / 2m^* \approx 0$ can be transmitted resonantly, where m^* denotes effective electron mass in GaAs. This explains the observed magnetic-field dependence: As long as the Fermi energy in the tip is below the $Al_xGa_{1-x}As$ barrier height, it will always be a constant number of electrons that tunnel resonantly, because the allowed energy regime for resonant tunneling is always the same in

$E_\parallel$ and independent of the Fermi energy in the tip. Thus, the corresponding BEEM current stays constant in this regime.

The oscillatory behavior of the BEEM spectra in magnetic fields can be explained in analogy to the Shubnikov de-Haas effect in two-dimensional electron-gas systems: In magnetic fields, Landau levels will exist inside the resonant tunneling diode. If the magnetic field is increased, the Landau-level spacing increases, too. Thus, the number of Landau levels inside the allowed $E_\parallel$ range will decrease. As each allowed Landau level carries a part of the BEEM current, a minimum in the BEEM current can be expected each time a Landau level is shifted outside the allowed $E_\parallel$ range. The minima will be equidistant in $1/B$ and in analogy to the Shubnikov de-Haas effect, the width of the allowed $E_\parallel$ range is determined by:

$$\Delta E_\parallel = \frac{e\hbar}{m^* \Delta\left(\frac{1}{B}\right)}, \qquad (3)$$

where $m^* = 0.067 m_0$ is the GaAs effective mass, and $\Delta(1/B) = 1/B_n - 1/B_{n+1}$ is the distance between two adjacent minima in the BEEM current as a function of magnetic field.

If we look at the data in Fig. 8(b), we observe three clear minima for the curve obtained at $V_t = 1.25$ V and two minima for the curve obtained at $V_t = 1.15$ V. Inserting the minima position in the above relation yields a filter width of $E_\parallel(1.25$ V$) = 13$ meV and $E_\parallel(1.15$V$) = 11$ meV. This indicates that the filter width increases with increasing STM bias, but a detailed dependence of $E_\parallel(V_t)$ cannot be extracted, because the signal to noise ratio is presently not good enough.

Finally, the width of the calculated current distribution can be compared with the values obtained from the magnetic field data. If the full width at half maximum value is taken for a bias of 1.14 V a value of $\mathbf{k}_\parallel = 0.17$ nm^{-1} is obtained. This corresponds to an $E_\parallel$ value of 16 meV, which is in reasonably good agreement with the experimental result from the Shubnikov de-Haas (SDH) oscillations of 11 meV at a value of $V_t = 1.15$ V, in particular if the simplicity of our model assumption is taken into account.

V. CONCLUSION

BEEM spectra for GaAs/$Al_xGa_{x-1}As$ DBRTD's have been calculated in terms of an atomistic Landauer-Büttiker-type scattering approach as well as measured for different GaAs cap layers. In accordance with earlier findings,[1] the steplike features in the spectrum for GaAs caps of about 4 nm were theoretically attributed to a parallel wave-vector $\mathbf{k}_\parallel$ filtering effect due to states localized at the alloyed interface. The latter are induced by Au interstitials in the first two GaAs ML. For an idealized Au/GaAs interface, the calculations yield a linear increase irrespective of the cap thickness. Furthermore, the step vanishes for the alloyed interface if a cap layer of 10 nm or larger is assumed. This can be explained in terms of a decoupling of the localized states at the

intermixed Au/GaAs interface and the quasibound state of the resonance.

To confirm this assertion, magnetic-field dependent BEEM studies were carried out on RTD's grown directly below the sample surface. The steplike features in the BEEM spectra exhibit a Shubnikov de-Haas-like oscillating behavior in strong magnetic fields. Both the step and the magnetic-field dependence are not observed for RTD's buried 10 nm below the surface. The filter width from the calculations agrees well with the results estimated from the SDH oscillations.

*Electronic address: Strahberger@wsi.tum.de

†Electronic address: Juergen.Smoliner@tuwien.ac.at

[1] J. Smoliner, R. Heer, and G. Strasser, Phys. Rev. B **60**, 5137 (1999).

[2] D.L. Smith, E.Y. Lee, and V. Narayanamurti, Phys. Rev. Lett. **80**, 2433 (1998).

[3] L.D. Bell, Phys. Rev. Lett. **77**, 3893 (1996).

[4] W.J. Kaiser and L.D. Bell, Phys. Rev. Lett. **60**, 1406 (1988).

[5] L.D. Bell and W.J. Kaiser, Phys. Rev. Lett. **61**, 2368 (1988).

[6] W.J. Kaiser, M.H. Hecht, L.D. Bell, F.J. Grunthaner, J.J. Liu, and L.C. Davis, Phys. Rev. B **48**, 18 324 (1993).

[7] H. Sirringhaus, E.Y. Lee, and H. von Knel, Phys. Rev. Lett. **73**, 577 (1994).

[8] R. Ludeke, M. Prietsch, and A. Samsavar, J. Vac. Sci. Technol. B **9**, 2342 (1991).

[9] M. Prietsch and R. Ludeke, Phys. Rev. Lett. **66**, 2511 (1991).

[10] E.Y. Lee, S. Bhargava, M.A. Chin, and V. Narayanamurti, J. Vac. Sci. Technol. A **15**, 1351 (1997).

[11] E.Y. Lee, S. Bhargava, K.J. Pond, K. Lou, M.A. Chin, and V. Narayanamurti, Appl. Phys. Lett. **69**, 949 (1996).

[12] X.C. Cheng, D.A. Collins, and T.C. McGill, J. Vac. Sci. Technol. A **15**, 2063 (1997).

[13] R. Landauer, IBM J. Res. Dev. **32**, 306 (1988).

[14] M. Büttiker, IBM J. Res. Dev. **32**, 317 (1988).

[15] J.N. Schulman and Y.C. Chang, Phys. Rev. B **27**, 2346 (1983).

[16] J.N. Schulman and D.Z.-Y. Ting, Phys. Rev. B **45**, 6282 (1992).

[17] D.Z.-Y. Ting, E.T. Yu, and T.C. McGill, Phys. Rev. B **45**, 3583 (1992).

[18] T.B. Boykin, Phys. Rev. B **54**, 7670 (1996).

[19] K. Reuter, P.L. de Andres, F.J. Garcia-Vidal, D. Sestovic, F. Flores, and K. Heinz, Phys. Rev. B **58**, 14 036 (1998).

[20] F.J. Garcia-Vidal, P.L. de Andres, and F. Flores, Phys. Rev. Lett. **76**, 807 (1996).

[21] C. Strahberger and P. Vogl, Phys. Rev. B **62**, 7289 (2000).

[22] W. A. Harrison, *Elementary Electronic Structure* (World Scientific, Singapore, 1999).

[23] J.-M. Jancu, R. Scholz, F. Beltram, and F. Bassani, Phys. Rev. B **57**, 6493 (1998).

[24] D. A. Papaconstantopoulos, *Handbook of the Band Structure of Elemental Solids* (Plenum Press, New York, 1986).

[25] M. Graf and P. Vogl, Phys. Rev. B **51**, 4940 (1995).

[26] Aldo Di Carlo, P. Vogl, and W. Pötz, Phys. Rev. B **50**, 8358 (1994).

[27] J.J. O'Shea, T. Sajoto, S. Bharagava, D. Leonard, M.A. Chin, and V. Narayanamurti, J. Vac. Sci. Technol. B **12**, 2625 (1994).

[28] M.-L. Ke, D.I. Westwood, C.C. Matthai, B.E. Richardson, and R.H. Williams, Phys. Rev. B **53**, 4845 (1996).

[29] J.J. O'Shea, E.G. Brazel, M.E. Rubin, S. Bhargava, M.A. Chin, and V. Narayanamurti, Phys. Rev. B **56**, 2026 (1997).

[30] D.L. Smith, M. Kozhevnikov, E.Y. Lee, and V. Narayanamurti, Phys. Rev. B **61**, 13 914 (2000).

[31] D.L. Smith and Sh.M. Kogan, Phys. Rev. B **54**, 10 354 (1996).

[32] W.J. Kaiser, L.D. Bell, M.H. Hecht, and F.J. Grunthaner, J. Vac. Sci. Technol. B **7**, 945 (1989).

[33] A.A. Talin, D.A.A. Ohlberg, R.S. Williams, P. Sullivan, I. Koutselas, B. Williams, and K.L. Kavanagh, Appl. Phys. Lett. **62**, 2965 (1993).

[34] R.M. Charatan and R.S. Williams, J. Appl. Phys. **72**, 5226 (1992).